Dielectric, electro-optical, and photoluminescence characteristics of ferroelectric liquid crystals on a graphene-coated indium tin oxide substrate

Dharmendra Pratap Singh, Swadesh Kumar Gupta, Tripti Vimal, and Rajiv Manohar*
Liquid Crystal Research Lab, Physics Department, University of Lucknow, Lucknow 226007, India
(Received 21 March 2014; published 18 August 2014)

Multilayer graphene was deposited on indium tin oxide (ITO) -coated glass plates and characterized by suitable techniques. A liquid crystal sample cell was designed using graphene deposited ITO glass plates without any additional treatment for alignment. Ferroelectric liquid crystal (FLC) material was filled in the sample cell. The effect of multilayer graphene on the characteristics of FLC material was investigated. The extremely high relative permittivity of pristine graphene and charge transfer between graphene and FLC material were consequences of the enormous increase in relative permittivity for the graphene-FLC (GFLC) system as compared to pure FLC. The presence of multilayer graphene suppresses the ionic impurities, comprised in the FLC material at lower frequencies. The ionic charge annihilation mechanism might be responsible for the reduction of ionic impurities. The presence of graphene reduces the net ferroelectricity and results in a change in the spontaneous polarization of pure FLC. Rotational viscosity of the GFLC system also decreases due to the strong π-π interaction between the FLC molecule and multilayer graphene. The photoluminescence of the GFLC system is blueshifted as compared to pure FLC, which is due to the coupling of energy released in the process of charge annihilation and photon emission.

DOI: 10.1103/PhysRevE.90.022501 PACS number(s): 42.70.Df, 77.22.Gm, 78.20.Jq, 68.65.Pq

I. INTRODUCTION

Research in the field of liquid crystals (LCs) is rapidly growing due to their spectacular properties [1–3]. The properties were initiated with display applications and nowadays, cover almost all the fields of science and technology [4–6]. The nature of LC or mesophase usually combines the physical and chemical properties of these materials and provides a wide field for technologists to develop devices and applications [7–9]. The chiral smectic-*C* (Sm*C**) mesophase has proven its potential among all other mesophases by showing faster response of microseconds order, better optical contrast and memory behavior [10–12]. At present, most of the displays are based on nematic, twisted nematic, and supertwisted nematic LCs [13,14], but the use of color filters, polarizers, and backlight source are compulsory parts of these displays [15]. Ferroelectric liquid crystals (FLCs) have also proven their potential as display materials. Some basic problems with this class of material (viz., bookshelf or chevron layer configuration, polar nature appearance of shadow pictures, etc.) make them less useful as display materials [16,17]. For display purposes, the LC molecules are fabricated on indium tin oxide (ITO) -coated glass sheets with a preferred alignment [17]. The perfect alignment of LC molecules on the alignment layer-coated ITO plates is also a difficult task and a number of studies have been reported to develop alignment methodology for the LC molecules [18–20].

Graphene is a two-dimensional zero band gap semiconductor having linear energy dispersion. It is a one-atom-thick layer of graphite discovered experimentally by Geim *et al.* [21]. Because of its outstanding electronic and optical properties, graphene has quickly attracted the interest of researchers and technologists during the last decade [22–25]. When electrons are confined in two-dimensional (2D) materials, quantum mechanically enhanced transport phenomena, as exemplified by the quantum Hall effects (QHEs), can be observed. Graphene is an ideal realization of such a 2D system. The FLCs are composed of tilted smectic mesophase and the chiral molecules. The tilt of the molecules is coupled to the layer thickness producing local biaxiality in the medium. Due to the chirality of the molecules, the mirror symmetry in the system leads to the possibility of sustaining an electric polarization (P), along the local twofold axis, spiraling uniformly about the twist axis of the helical structure. Therefore, the effect of a two-dimensional solid on a two-dimensional liquid (as FLCs are two-dimensional liquids) has been analyzed in the present investigation for dielectric, electro-optical, and photoluminescence applications.

The use of graphene and graphene derivatives in LCs imparts a new perspective for liquid crystal research to enhance a variety of properties [26–29]. During the last few years, various aspects of LCs with graphene have been reported for the understanding of graphene based LC composites [30–32]. The data of graphene based LC devices evince a new dimension in LC applications [33]. Nowadays, the symbiosis of graphene and LCs arouses rapidly increasing interest. In spite of this, only limited numbers of research articles on graphene-LC composites are reported in the literature. These reports explain the effect of graphene as a guest material on the various properties of host LCs. These reports are also limited to the nematic, discotic, and polymer LCs.

In the present article, we report the interaction of FLC material with multilayer graphene at the graphene-coated ITO substrate–FLC interface. These interfacial interactions between graphene-coated ITO substrate and FLC would be different from those of the graphene-LC composites reported in the literature. The multilayer graphene was first deposited on the ITO-coated glass plates and the FLC molecules were

*Corresponding author: rajiv.manohar@gmail.com

deposited over it without using any preferred alignment. The capacitor-type sample cell [34] was prepared with the help of multilayer graphene-coated ITO glass plates. An alignment layer was not used in the present investigation in order to study the interaction of FLC molecules with the deposited multilayer graphene whereas in the study of pure FLC, an alignment layer of nylon 6/6 was used to align the FLC molecules. We have also checked the role of multilayer graphene as an alignment layer for the FLC molecules. FLC molecules adopt the homogeneous (planar) alignment on the multilayer graphene which suggests that the multilayer graphene can also be used as a planar anchored alignment layer. The physical properties of the FLC material are found to be altered when deposited over the multilayer graphene. On multilayer graphene, the FLC material shows reduced spontaneous polarization and rotational viscosity whereas the optical response becomes slower. The relative permittivity of the FLC material on the multilayer graphene increases enormously due to the high relative permittivity of pristine graphene and charge transfer phenomenon between the graphene layers and FLC material. The ionic impurities associated with FLC material, which are more visible at lower frequencies, have been reduced due to the presence of multilayer graphene. The reduction of ionic impurities was further verified by the ac conductivity measurement. The reduced ionic impurities and enhanced relative permittivity of the FLC material on multilayer graphene suggest its use in the LC based dielectric devices with enhanced efficiency. The photoluminescence property of the FLC material on the multilayer graphene was also carried out for analyzing the use of the present system in the optical and display devices. As graphene can be coated on a flexible substrate, therefore, the use of graphene for the development of a transparent flexible LC display is the main assumption of the present study. In brief, the presence of graphene at the FLC-ITO interface; its effect on the electro-optical, dielectric, and photoluminescence properties of pristine FLC; and the role of graphene as alignment material are the main motives of this investigation.

II. EXPERIMENT

A. FLC material

The FLC material used in the present study is FELIX 16/100. It is a commercial FLC mixture purchased from Clariant Chemicals Co. Ltd., Germany. The phase sequence of FLC material is as follows:

$$\mathrm{Cry} \xrightarrow{20\ ^\circ\mathrm{C}} \mathrm{Sm}C^* \xrightarrow{72\ ^\circ\mathrm{C}} \mathrm{Sm}A \xrightarrow{82\ ^\circ\mathrm{C}} N^* \xrightarrow{90\ ^\circ\mathrm{C}-94\ ^\circ\mathrm{C}} I.$$

B. Photolithography for developing the active area on indium tin oxide (ITO) -coated glass plates

ITO-coated optical flat glass plates have been imported from Diamond Coatings (UK). The sheet resistance and visible light transmission of the ITO sheets was 10 Ω/cm^2 and 90%, respectively. The rectangular pattern on the ITO-coated glass plate was achieved by the photolithographic technique. The ITO-coated glass plates were cleaned by soap solution and acetone with the help of an ultrasonic cleaner to avoid any traces of organic impurities and dust particles. The cleaned ITO glass plates were dried in a hot air oven for 30 min. We applied negative photoresist (Sigma-Aldrich, Product No. 651796) on the ITO-coated glass plates by the spin coating technique for a period of 5 min at a speed of 4000 rpm. The negative photoresist–coated ITO glass plates were dried at 90 °C for 1 h and then exposed to UV light using a rectangular photomask. The rectangular pattern (also called the *active area*) was developed by suitable developer. Further, the developed pattern was baked at 220 °C for 3 h. The baking at 220 °C causes hardening in the developed active area. The extra ITO rather than the active area was removed by the etching process using zinc dust and dilute hydrochloric acid (HCl). The active area was $0.5 \times 0.5\ \mathrm{cm}^2$. The plates were again cleaned by soap solution and acetone. After this stage, we proceed to deposit the graphene on the active area.

C. Deposition of multilayer graphene on ITO surface and its characterization

A top-to-bottom approach was adopted to deposit the multilayer graphene on the active area of the ITO surface. The graphitic powder was purchased from Graphene Research Ltd., Manchester, UK. This graphitic powder was exfoliated by sonication in dimethylformamide (DMF) for 2 h. DMF dissolves graphite and results in a suspension of thin graphitic platelets with a large proportion of graphene flakes. The suspension was centrifuged for 30 min at 7000–9000 rpm. This suspension of graphene was spin coated over the active area of dimensions $1 \times 1\ \mathrm{cm}^2$ which consists of overlapped individual graphene and a few layers of graphene flakes. The graphene-coated ITO glass plates were annealed for 3 h in inert atmosphere at 250 °C. This process is already discussed by Blake *et al.* [33] in detail. The presence of multilayer graphene reduces the transmittance of pristine ITO-coated glass plates by ≈20%. The deposition of a transparent graphene layer on the ITO-coated glass plates is a task that would be needed in order to fabricate transparent display devices. Using this approach, the development of stretchable transparent electrodes made of graphene film has been reported recently [35]. The transmittance of ITO is usually 2.3% lower when a monolayer graphene covers it. This lowering in the percentage transmittance due to the presence of a graphene layer has already been reported by Nair *et al.* [36]. The transparency of graphene only depends on the fine structure constant ($\alpha = 2\pi e^2/hc$), where e is the charge on the electron, h is Planck's constant, and c is the speed of light. The fine structure constant (α) explains the coupling between light and a relativistic electron. The absorbance of white light increases linearly with the number of graphene layers from one to five; therefore, the absorbance of n layers of graphene can be simply expressed as $n\pi\alpha$ [37]. In the present study, the presence of almost ten graphene layers on the ITO surface was confirmed by the UV-visible absorption spectroscopy.

The graphene was deposited on the ITO surface with a motive to observe the role of graphene as alignment material on the ITO. As FLC molecules adopt the homogeneous alignment over the multilayer graphene, this certifies the role of graphene as planar anchored alignment material for the FLC molecules. Several characterization techniques were used to probe the confirmation of multilayer graphene on the active area of

ITO-coated glass plates. Raman spectroscopy (Model Alfa 300, WITec GmbH, Germany) and x-ray diffraction (XRD) (Model Bruker D8 Advance x-ray diffractometer) for 2θ values ranging from 5 ° to 90 ° using Cu$K\alpha$ radiation (λ = 1.5418 Å)] were used to characterize the deposited multilayer graphene. The surface morphology of multilayer graphene was performed by scanning electron microscopy (SEM) (Model No. LEO-430, Make-LEO, Cambridge, UK). The absorbance of white light by the multilayer graphene, for estimating the number of graphene layers on the ITO surface was performed on a UV-VIS spectrophotometer (ELICO, Model No. SL201) for the wavelength interval of 300–1100 nm.

D. Preparation of sample cell and measurements

The multilayer graphene-coated ITO glass plates were assembled into the capacitor-type sample cell. The uniform thickness (5 μm in the present case) of the sample cells was maintained by means of a Mylar spacer. The fabrication of the sample cell with the help of the multilayer graphene-coated ITO is shown in Fig. 1. The arrangement of FLC molecules deposited on the multilayer graphene/ITO is termed as graphene-FLC (GFLC). The analysis of pure FLC has been carried out on the ITO surface with an alignment layer of polyamide (nylon 6/6) and is referred to as the pure FLC in the paper for the sake of simplicity, whereas in the GFLC system, multilayer graphene was deposited on ITO without using any polyamide layer. The empty sample cells were calibrated using analytical reagent (AR) grade carbon tetrachloride (CCl_4) and benzene (C_6H_6). Detailed information about the preparation of the sample cell using a polyamide layer has already been reported by our group [38]. The FLC material was filled in the multilayer graphene-coated sample cell in the isotropic phase by means of capillary action and then cooled gradually down to room temperature. The alignment of samples was checked by a polarizing optical microscope under the crossed polarizer-analyzer arrangement. The polarizing optical micrographs were taken by a polarizing optical microscope, RXLr-5 (Radical, India), at room temperature.

The dielectric spectroscopy of pure FLC (ITO + nylon 6/6 as alignment layer) and GFLC (ITO + multilayer graphene) was performed on a computer controlled Impedance/Gain-Phase analyzer (HP4194A). The dielectric measurements were carried out as a function of temperature by placing the sample cell on a computer controlled hot plate (Instec, HCS 302, USA). The temperature stability was better than ±0.1 °C. Dielectric spectroscopy was performed for the frequency range of 100 Hz to 1 MHz.

The spontaneous polarization (P_S) measurement was performed using a polarization reversal method [39]. The triangular wave signal of voltage $20V_{\text{P-P (peak to peak)}}$ and frequency of 10 Hz were applied across the sample cell with the help of a programmable function generator (Tektronix AFG 3021B) and the output electrical response was recorded on the oscilloscope (Tektronix TDS 2024C).The P_S was determined by using the following relation [40]:

$$P_S = \frac{1}{2A}\int i(t)dt, \tag{1}$$

where $\int i(t)dt$ is the area under the current bump and A is the active area of the sample cell.

For the measurement of optical response time (τ_{Res}), a square wave signal of 10 Hz and $20V_{\text{P-P}}$ was applied across the sample cell. He-Ne laser (5 mW power and wavelength 633 nm) was used as the optical source and the output response was recorded by a photodetector (PD02, Instec, U.S.A.). The response time was calculated by using the following relation [41]:

$$\tau_{\text{Res}} = \frac{t_{10} - t_{90}}{1.8}, \tag{2}$$

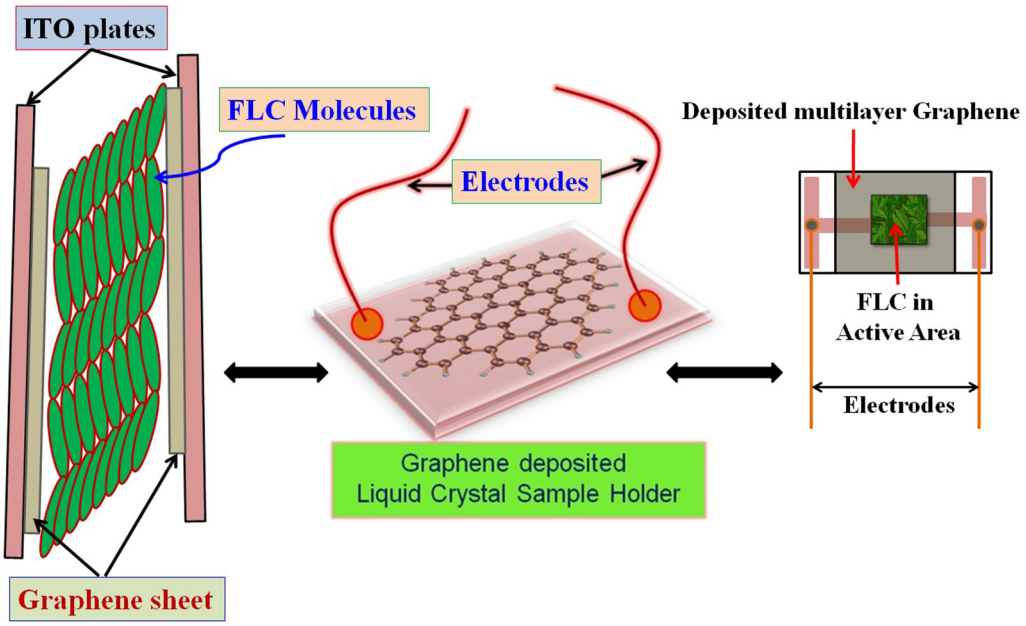

FIG. 1. (Color online) The diagram for the fabrication of a liquid crystal sample cell with the help of multilayer graphene-coated ITO glass plates.

where t_{10} and t_{90} are the corresponding times for 10% and 90% transmission from the maximum level of response time.

The photoluminescence (PL) spectra of the pure FLC and GFLC system were recorded using Perkin Elmer LS 55 luminescence spectrophotometer equipped with a xenon discharge lamp of power equivalent to 20 kW for 8 ms duration as the excitation source at room temperature. During the PL measurement, all the measuring parameters such as slit width (4 nm in our case), excitation step, etc., were the same for both systems. The excitation wavelength was 310 nm for the PL measurement.

III. RESULTS AND DISCUSSION

Raman spectroscopy is a very sensitive and useful technique to characterize the carbon atoms in the sp^2 or sp^3 hybridization state. The various signatures of graphene (viz., single layer, double layer, or multilayer graphene) are differentiated by the Raman spectra. In order to characterize the deposited multilayer graphene, the Raman spectrum was recorded using 514-nm excitation wavelength and is shown in Fig. 2(a). The G, D' and $2D$ bands were clearly observed at 1522, 1556, and 2675 cm^{-1}. The stretching of the C-C bond in graphitic materials results in the G band which is very common in sp^2 hybridized carbon atoms. The presence of surface charges or randomly distributed dipoles (or randomly distributed impurities) causes the splitting of the G band. The splitting of the G band results in the formation of the D' band at 1556 cm^{-1} as a signature of the presence of surface charges on the deposited multilayer graphene. The broad $2D$ band was also observed at 2675 cm^{-1}. The relative profiles of G and $2D$ bands indicates the presence of multilayer graphene on the active area of ITO-coated glass plates. The Raman study of the deposited graphene confirms the presence of multilayer graphene with additional surface charges. We have not observed any evidence of an ITO peak in the Raman spectrum which proves that the multilayer graphene is almost uniformly deposited over the active area of the ITO.

The XRD spectrum of deposited multilayer graphene is shown in Fig. 2(b). A broad diffuse peak associated with the (002) plane was observed at 22.04 ° on the 2θ scale. The presence of a diffuse peak associated with the (002) plane at 22.04 ° proves that the graphene is present on the active area of the ITO surface [42]. The surface morphology of the deposited multilayer graphene was analyzed by the SEM study. The SEM image of the deposited multilayer graphene on the ITO surface is shown in Fig. 2(c). An example of the graphene layer is inserted as an inset of Fig. 2(c) which almost coincides with the SEM image of the deposited multilayer graphene. The SEM image elucidates the deposition of multilayer graphene on the ITO surface. Some turbulent traces in the SEM image may be due to the presence of

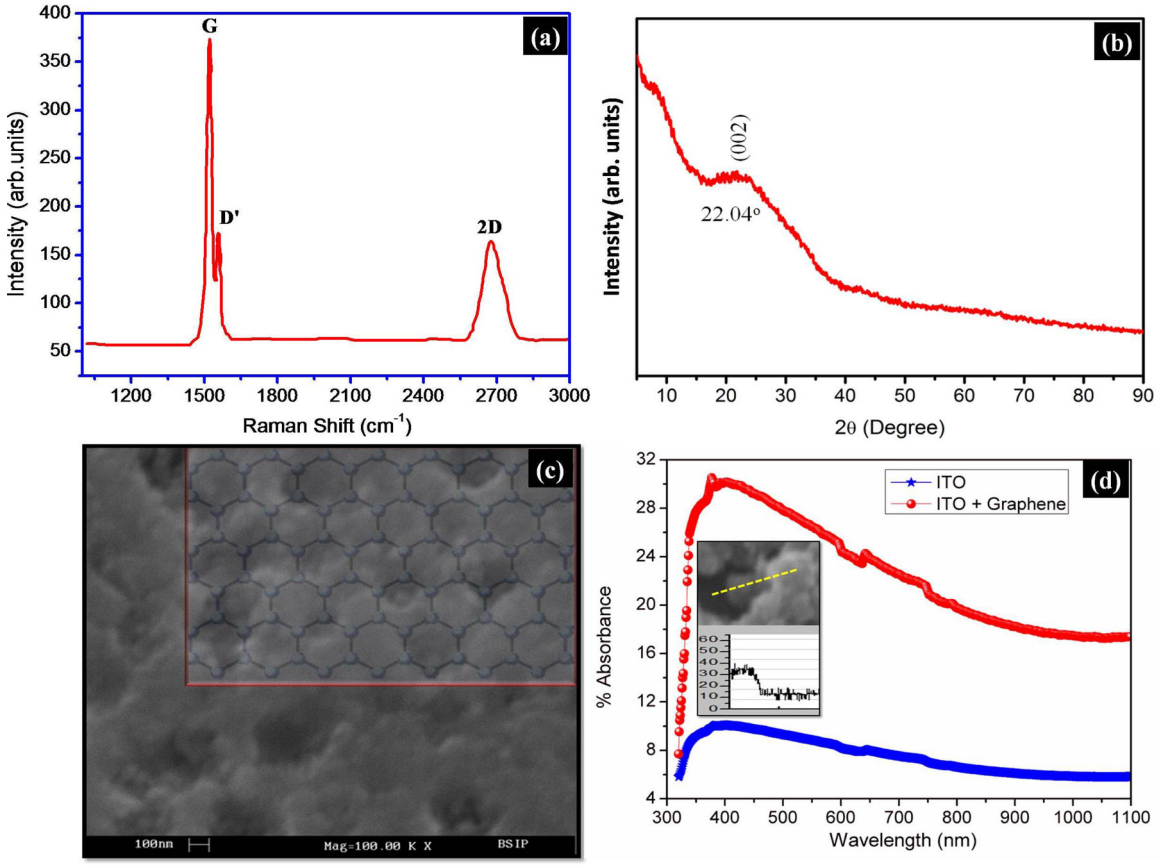

FIG. 2. (Color online) The characterization of deposited multilayer graphene by (a) Raman spectrum, (b) x-ray diffraction (XRD) spectrum, (c) scanning electron microscopic (SEM) image, and (d) UV-visible absorbance spectrum. The inset of (d) shows the absorption profile estimated from the SEM image at the dark-bright region.

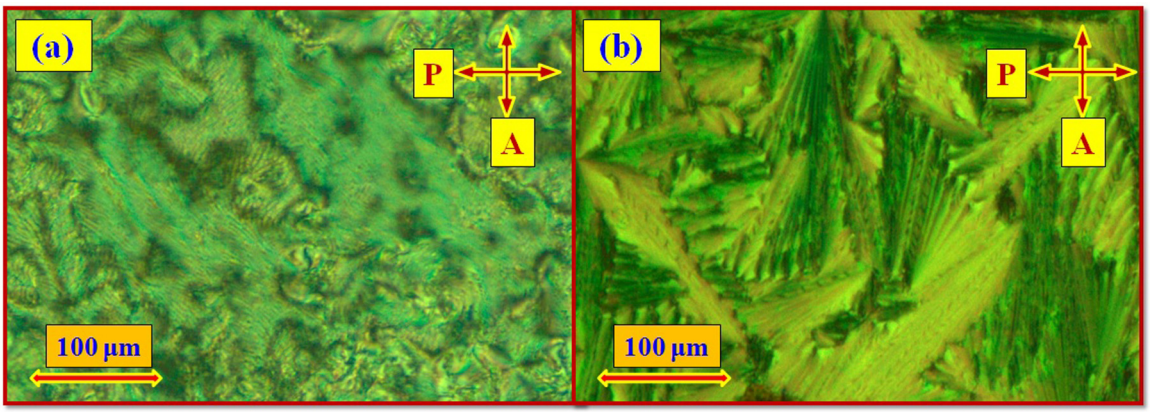

FIG. 3. (Color online) The polarizing optical micrographs of (a) pure FLC and (b) GFLC system under crossed polarizer conditions at 35 °C.

surface charges on the multilayer graphene. The presence of surface charges has already been confirmed by the Raman spectrum.

The UV-visible absorption spectroscopy, shown in Fig. 2(d), was carried out to impart the number of graphene layers on the ITO surface. As the presence of single layer graphene absorbs the 2.3% of incident light, therefore the absorbance of ≈20% of incident light by the multilayer graphene deposited ITO surface, as compared to pristine ITO surface, confirms the presence of almost ten layers of graphene on the ITO surface. The inset of Fig. 2(d) shows the absorption profile (estimated from the SEM image) of the multilayer graphene deposited ITO glass plates. The absorption profile of the SEM image also supports the result of the UV-visible absorption measurement and confirms the presence of ten graphene layers on the ITO surface.

Figures 3(a) and 3(b) demonstrate the polarizing optical micrographs of pure FLC and GFLC, respectively. The micrographs were taken at room temperature. It is clear from the micrographs that the pure FLC possesses schlieren texture whereas the paramorphotic broken focal-conic fan texture was observed for the GFLC system. Therefore, the optical micrographs of both systems reveal the homogeneous patterning on the polyamide layer and multilayer graphene. In spite of this homogeneity, a drastic change in the optical micrographs suggests that the molecular ordering of FLC molecules on the multilayer graphene in comparison to that of the polyamide layer has been changed significantly. It also indicates that the helical structure of FLC molecules has been perturbed on the multilayer graphene due to the presence of randomly distributed dipoles on the surface of the graphene.

The variation of relative permittivity on the frequency scale for pure FLC and GFLC at different temperatures (40 °C–60 °C) is depicted in Figs 4(a) and 4(b), respectively. A similar trend of relative permittivity with the change in frequency has been observed for both systems with a significant change in magnitude. On increasing the frequency, the relative permittivity of both systems (pure FLC and GFLC) decreases due to the phase lag between the motion of FLC molecules and applied frequency. The magnitude of relative permittivity for the GFLC system is enormously high as compared to pure FLC. The relative permittivity of the GFLC system is found to be ten- and 12-fold that of the pure FLC measured at 200 and 500 Hz, respectively. This tremendous increase in relative permittivity for the GFLC system in comparison to pure FLC may be due to two reasons. The first reason is the charge transfer between multilayer graphene and FLC material. The extremely high relative permittivity of pristine graphene (Supplemental Material [43]) is the second reason which influences the relative permittivity of pure FLC material. The insets of Figs. 4(a) and 4(b) show the change in relative permittivity on the temperature scale measured at 200 and 500 Hz for the pure FLC and GFLC system, respectively. It is clear from the insets that the relative permittivity of the GFLC system slightly increases with increasing temperature and falls sharply near the SmC^*-SmA phase transition temperature as compared to pure FLC. Figure 4(c) shows the variation of tanδ ($\varepsilon''/\varepsilon'$, the ratio of imaginary and real parts of the complex dielectric permittivity) at 40 °C on the frequency scale for pure FLC and GFLC systems. Due to phase angle fluctuations the Goldstone mode of relaxation is clearly observed near 300 Hz for pure FLC and GFLC systems. At lower frequencies, the magnitude of tanδ for the GFLC system is less as compared to the pure FLC. This is due to the suppression or reduction of ionic impurities of the FLC material at lower frequencies in the presence of multilayer graphene. Another reason for the decrement of the ionic impurities associated with FLC material at lower frequencies may be the ionic charge annihilation. When FLC material is present on the multilayer graphene, the ionic impurities of FLC material combine with the surface charges associated with multilayer graphene and annihilate each other due to their opposite natures. Due to the ionic charge annihilation process, the effect of ionic impurities for the GFLC system has been reduced. The ionic impurities impair the physical properties of FLC materials at lower frequencies and thus degrade the practical applications of FLC materials. Therefore, the GFLC system can be used as ionic impurity–free functional material for FLC based dielectric devices. In addition to this, the Goldstone relaxation mode becomes wider for the GFLC system. The widening of the Goldstone mode of relaxation is due to the molecular hindrance in the dynamics of FLC molecules on the multilayer graphene surface. The reduction of ionic impurities was also confirmed by measuring the ac conductivity for both systems. The variation of ac

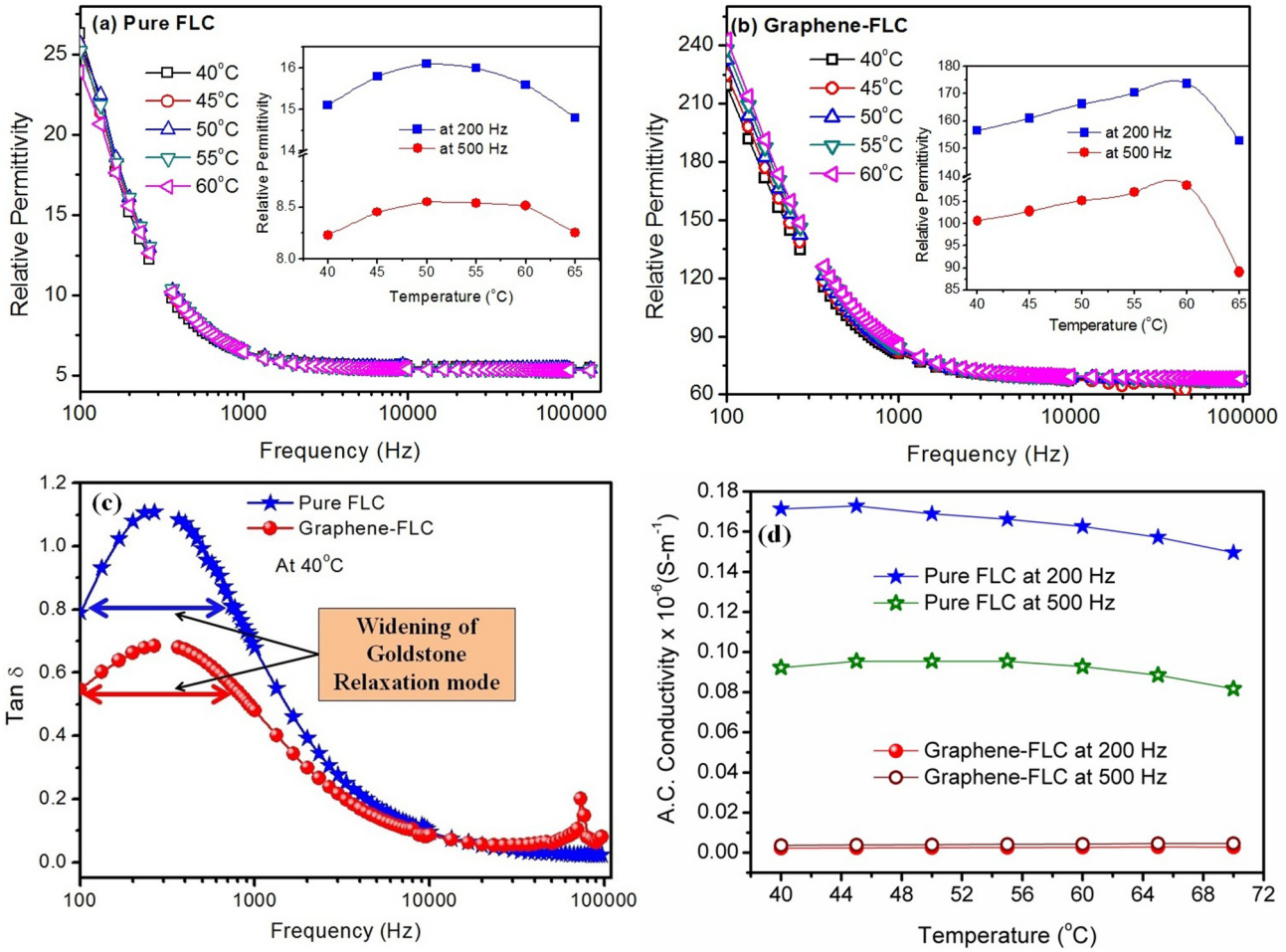

FIG. 4. (Color online) The variation of relative permittivity of (a) pure FLC and (b) graphene-FLC on the frequency scale for different temperatures (40 °–60 °C), whereas (c) represents the variation of tanδ ($\varepsilon''/\varepsilon'$) at 40 °C on the frequency scale and (d) shows the variation of ac conductivity with the change in temperature for pure FLC and graphene-FLC at 200 and 500 Hz. The insets of (a) and (b) represent the variation of relative permittivity of pure FLC and GFLC systems with the change in temperature at 200 and 500 Hz, respectively.

conductivity, at 200 and 500 Hz, for pure FLC and GFLC systems, has been presented in Fig. 4(d). It is clear from the figure that the ac conductivity of the GFLC system (at 200 and 500 Hz) is lower as compared to the pure FLC system which interprets the reduction of ionic impurities. Graphene shows conductivity without charge carriers, which is also known as graphene's zero-field conductivity. This quantized conductive property of the graphene provides a better platform for the phenomenon of charge transportation [44].

The change in polarization, at 35 °C, for the FLC material on the bias voltage scale with polyamide/ITO and multilayer graphene/ITO surface is depicted in Fig. 5(a). The polarization of the FLC material is voltage dependent and increases with increasing bias voltage. At higher bias voltage, the value of polarization saturates, which is the value of spontaneous polarization (P_S) for FLC material. It is clear from Fig. 5(a) that the value of spontaneous polarization of FLC material on the multilayer graphene/ITO surface is almost half as compared to pure FLC on the polyamide layer. The randomly distributed local dipoles associated with the multilayer graphene reduce the effective ferroelectricity of GFLC system as compared to pure FLC. The spontaneous polarization and rotational viscosity of the FLC material are related to each other as follows [45]:

$$P_S = \frac{\gamma_d}{\tau_{\mathrm{Res}} E}, \tag{3}$$

where γ_d and E are the rotational viscosity and applied field on the active area, respectively. The rotational viscosity was calculated using the above-mentioned Eq. (3).

The change in rotational viscosity for pure FLC and GFLC systems on the bias voltage scale is shown in Fig. 5(b). The reduction of rotational viscosity for the GFLC system is probably due to the strong π-π interactions between the multilayer graphene and FLC molecules. This reduction in the rotational viscosity is analogous to the reduced value of spontaneous polarization for GFLC system.

The optical response time, at 35 °C, on the bias voltage scale for pure FLC and GFLC systems is depicted in Fig. 6. A slower optical response for the GFLC system compared with that of the pure FLC system has been observed. The repercussion of the variation of optical response time on the bias voltage scale comprises the combined behavior of spontaneous polarization and rotational viscosity. The scuffling of randomly distributed

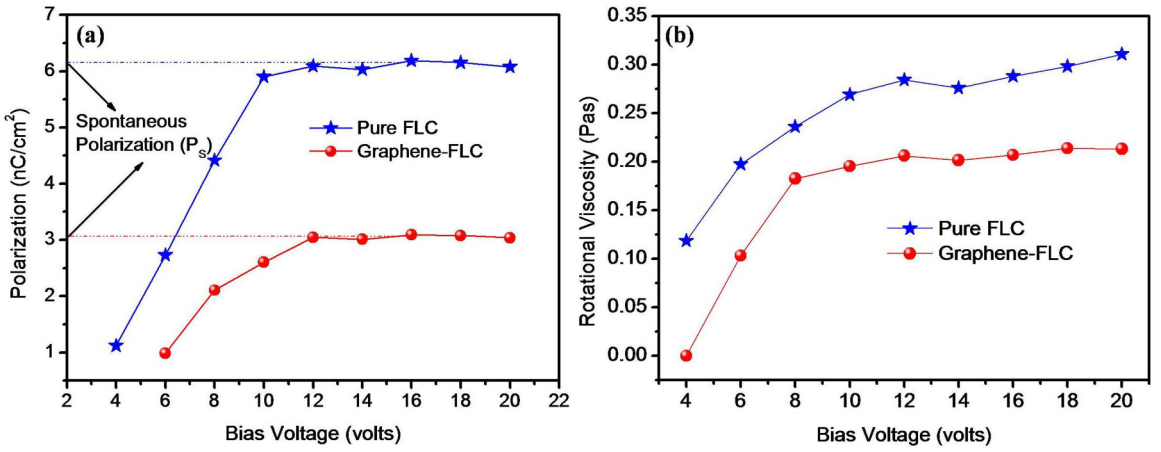

FIG. 5. (Color online) (a) Variation of polarization with the change in bias voltage for FLC material with and without the presence of multilayer graphene on the ITO surface at 35 °C. The saturation value of polarization on the bias voltage scale is the spontaneous polarization of the material. (b) represents the change in rotational viscosity as a function of bias voltage at 35 °C.

local dipoles present on the surface of multilayer graphene with the FLC molecules and strong π-π interaction (between the multilayer graphene and FLC molecules) obstruct the quick response of FLC molecules under the application of incident light of optical source. The FLC molecules can interact (or bind) with multilayer graphene through either the noncovalent interaction or chemical bonding. The scenario outlined above has been taken with a hypothesis that the FLC molecules interact with the multilayer graphene at the interface by π-π interaction which is very common in carbon based materials. These are the two main factors for the slower optical response of FLC molecules on the multilayer graphene surface.

The photoluminescence of pure FLC and GFLC systems using 310-nm excitation wavelengths (3.99 eV) is shown in Fig. 7(a). The inset of Fig. 7(a) shows the PL of the pure FLC excited with the same excitation wavelength. The PL emission peak for pure FLC material is centered at 388 nm (3.19 eV) whereas the GFLC system shows the primary PL emission peak at 377 nm (3.28 eV). It is clear from the figure that the

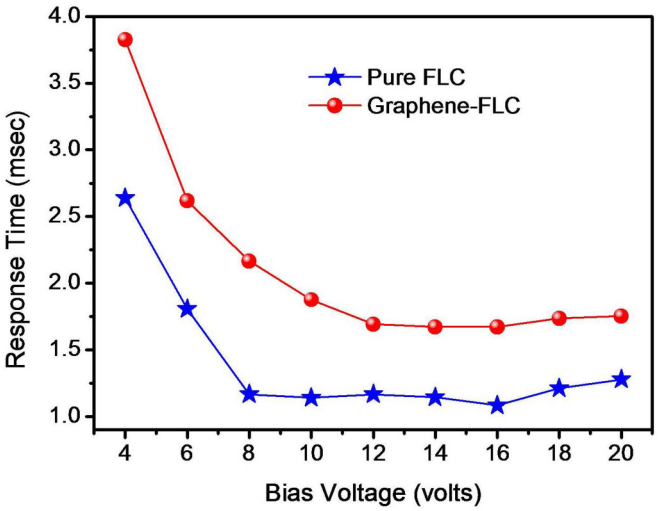

FIG. 6. (Color online) The behavior of response time on the bias voltage scale for the FLC material with and without the presence of multilayer graphene on the ITO surface at 35 °C.

PL of the GFLC system is blueshifted by 11 nm (0.09 eV) as compared to pure FLC. It is believed that the energy released in the process of charge annihilation couples with the photon emission. This coupling provides the emission of more energetic photons of energy 3.28 eV (377 nm) for the GFLC system as compared to the emitted photon of energy 3.19 eV (388 nm) associated with the pure FLC system. In addition to this, we have observed few secondary emission peaks in the PL spectrum of GFLC system. The asymmetric distribution of PL emission peaks on the wavelength scale implies that the FLC material on multilayer graphene does not produce a single PL emission. To deduce the possible number of emissions, we fitted the PL spectrum of the GFLC system by the Gaussian fit. The Gaussian fit of the PL emission is depicted in Fig. 7(b). The effect of PL emission associated with the pristine multilayer graphene has also been taken into account. The inset of Fig. 7(b) shows the PL emission of pristine multilayer graphene. The multilayer graphene posses two emission peaks at 484 and 530 nm, respectively. The intensity of the emission peak at 530 nm is feeble. Now, it is clear that the PL emission of the GFLC system also contains the PL emission of pristine multilayer graphene but it is slightly blueshifted. The PL emission peaks centered at 484 and 530 nm associated with pristine multilayer graphene were observed at 477 and 526 nm in the GFLC system, respectively. When multilayer graphene is treated with FLC material, the lateral shift in the valence and conduction bands of the multilayer graphene might be the reason for this blueshifting. The Gaussian fit reveals that the PL spectrum of the GFLC system is composed of four individual PL emission peaks centered at 371.5, 412, 477, and 526 nm. The emission peaks at 412, 477, and 526 nm are associated with the violet, blue, and green colors whereas the emission peak at 371.5 nm lies at the UV-near-visible region in the optical spectrum. The Gaussian profile of the PL spectrum for the GFLC system suggests the existence of four peaks that originated due to different processes. The radiation field couples with the surface plasmon present on the graphene layers which produces a high energy PL emission peak at 371.5 nm (3.33 eV). In the UV-visible absorption measurement [Fig. 2(d)], the maximum

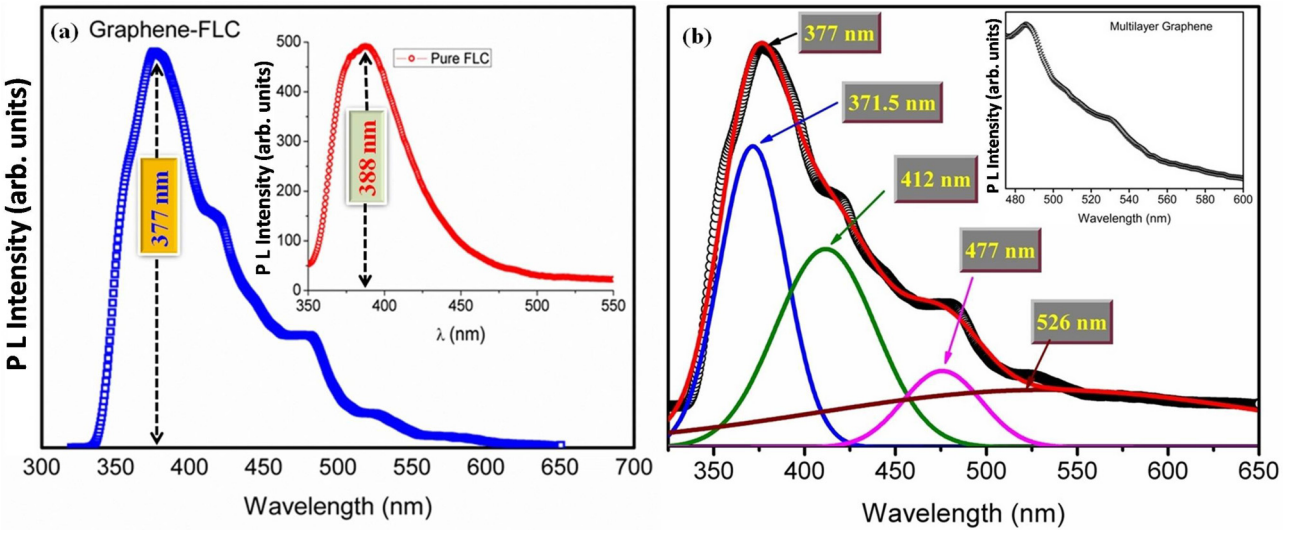

FIG. 7. (Color online) The variation of photoluminescence (PL) intensity on the wavelength scale for (a) graphene-FLC at room temperature (35 °C) and (b) the Gaussian fit of PL intensity curve to disclose the existence of the multiple peaks. The inset of (a) represents the PL intensity curve of the pure FLC whereas the inset of (b) shows the PL of pristine multilayer graphene. The excitation wavelength was 310 nm in the present investigation.

absorbance of incident light was observed at 412 nm for the multilayer graphene. This maximum absorbance of the incident light at 412 nm causes the broadening in the surface plasmonic mode. The broadening of the surface plasmonic mode produces an emission peak at 412 nm of violet color. During the charge transfer phenomenon between multilayer graphene and FLC, the recombination of electron-hole pair occurs at the interface of multilayer graphene and FLC which results in a PL emission at 477 nm corresponding to blue color. This PL emission peak is attributed to the pristine multilayer graphene (at 484 nm) but it is slightly blueshifted in the GFLC system. In the same pursuit, the PL emission peak at 526 nm for the GFLC system is also associated with the pristine multilayer graphene and it is also blueshifted. The reason for the blueshifting of the PL emission peaks has been discussed previously. Near the edges of multilayer graphene, broken symmetry of graphene causes the scattering of charges which produces the PL emission peak at 526 nm of green color. The coupling of the radiation field and surface plasmon, *e-h* pair recombination, and charge scattering in the graphene and graphene derivatives have already been reported [46–48]. The observed PL properties strongly suggest the use of a GFLC system in dual color (blue-green) light-emitting diodes (LEDs) and better photoluminescent display materials.

IV. CONCLUSIONS

The multilayer graphene was deposited on the active area of ITO-coated glass plates by the spin coating method. The deposited multilayer graphene was characterized by Raman spectroscopy, scanning electron microscopy (SEM), x-ray diffraction (XRD), and UV-visible absorption spectroscopy. The Raman spectroscopy and XRD confirm the presence of multilayer graphene on the ITO surface. The surface morphology of deposited multilayer graphene was carried out by SEM analysis. The presence of approximately ten graphene layers was confirmed by UV-visible absorption spectroscopy. The FLC molecules were deposited on a multilayer graphene/ITO surface without using any alignment layer. The use of an alignment layer is a compulsory process for aligning the LC molecules either in planar or homeotropic fashion. In the present study, we have not used any alignment layer on the ITO surface for disclosing the role of multilayer graphene as an alignment layer. As compared to a pure FLC system, the relative permittivity of a GFLC system increases enormously due to the charge transfer phenomenon between multilayer graphene and FLC material. The extremely high relative permittivity of pristine graphene may also be responsible for the enhanced relative permittivity of the GFLC system. The relative permittivity of both systems decreases with increasing frequency. The increment in the value of relative permittivity for the GFLC system was found to be ten- and 12-fold as compared to pure FLC measured at 200 and 500 Hz, respectively. The observed behavior of tanδ for the GFLC system suggests that the ionic impurities have been suppressed in the presence of multilayer graphene. The charge annihilation process may also be responsible for the reduced value of tanδ for the GFLC system. The reduction of spontaneous polarization for the GFLC system is attributed to the reduction of net ferroelectricity. The randomly distributed local dipoles or surface charges on the multilayer graphene reduce the effective dipole moment of the GFLC system which results in the lowered value of spontaneous polarization. The rotational viscosity of the GFLC system has also been reduced as compared to pure FLC due to strong π-π interaction between multilayer graphene and FLC molecules. The reduced value of rotational viscosity for the GFLC system is analogous to the lowered value of spontaneous polarization. The slower optical response has been observed for the GFLC system as compared to pure FLC. The slower optical response for the GFLC system is due to the combined change in the values

of spontaneous polarization and rotational viscosity. The photoluminescence of the GFLC system has been blueshifted as compared to the pure FLC system. The pure FLC and GFLC systems show PL emission peaks at 388 nm (3.19 eV) and 377 nm (3.28 eV), respectively. The more energetic PL emission from the GFLC system is due to the coupling between the released energy in the process of charge annihilation with that of the photon emission. It is also observed that the GFLC system produces few secondary PL emissions centered at 371.5, 412, 477, and 526 nm associated with UV-near-visible, violet, blue, and green colors, respectively. The secondary emission was estimated by the Gaussian fit of the PL spectrum. The origin of all secondary PL emissions has been explained. The observed optical properties of the GFLC system in PL measurement suggest the use of the present system in dual color LED and UV laser application. The development of the transparent electrodes of graphene and its deposition on the flexible substrate shows hope for the development of the transparent flexible LC display.

ACKNOWLEDGMENTS

The authors are thankful to the Department of Science and Technology, Government of India, for the financial assistance for the present work in the form of a project. We are also thankful to Mr. M. Mishra, Jawahar Lal University, New Delhi, for fruitful discussion and experimental help. We are also thankful to BSIP and IIT Kanpur for using the characterization facilities. The authors D.P.S. and S.K.G. are thankful to CSIR, India, for support from the SRF Grants No. 09/107(0363) 2012-EMR-I and No. 09/107(0337)2010-EMR-I, respectively. T.V. is thankful for support from UGC through a BSR fellowship. The authors are thankful to Professor Ivan I. Smalyukh (University of Colorado at Boulder, USA), Professor Mark Warner (Cavendish Laboratory, Cambridge University), and Professor T. Wilkinson (Engineering Department, Cambridge University) for support, encouragement, and suggestions for improvement of this work. D.P.S. is also thankful to CSIR, New Delhi, for providing the international travel support (Grant No. TG/7966/13-HRD).

[1] G. H. Brown, *Advances in Liquid Crystals* (Academic Press, London, 1976).
[2] M. Čopič, J. E. Maclennan, and N. A. Clark, Phys. Rev. E **65**, 021708 (2002).
[3] A. Kumar, J. Prakash, D. S. Mehta, A. M. Biradar, and W. Haase, Appl. Phys. Lett. **95**, 023117 (2009).
[4] J. A. Castellano, Liq. Cryst. Today **1**, 4 (1991).
[5] L. Calucci, G. Ciofani, D. D. Marchi, C. Forte, A. Menciassi, L. Menichetti, and V. Positano, J. Phys. Chem. Lett. **1**, 2561 (2010).
[6] F. V. Podgornov, A. M. Suvorova, A. V. Lapanik, and W. Haase, Chem. Phys. Lett. **479**, 206 (2009).
[7] J. L. Ericksen and D. Kinderlehree, *Theory and Applications of Liquid Crystals* (Springer-Verlag, London, 1987).
[8] Y. S. Ha, H. J. Kim, H. G. Park, and D. Shik, Opt. Express **20**, 6448 (2012).
[9] L. M. Blinov and V. G. Chigrinov, *Electrooptic Effects in Liquid Crystal Materials* (Springer, New York, 1996).
[10] J. S. Patel, Appl. Phys. Lett. **47**, 1277 (1985).
[11] H. Xu, S. M. Lughadha, A. Kocot, and J. K. Vij, Ferroelectrics **148**, 401 (1993).
[12] S. Kaur, A. K. Thakur, and A. M. Biradar, Appl. Phys. Lett. **88**, 122905 (2006).
[13] M. Schadt and W. Helfrich, Appl. Phys. Lett. **18**, 127 (1971).
[14] C. M. Watters and E. P. Raynes, Displays **8**, 59 (1987).
[15] J. J. Lyu, H. Kikuchi, D. H. Kim, J. H. Lee, K. H. Kim, H. Higuchi, and S. H. Lee, J. Phys. D: Appl. Phys. **44**, 325104 (2011).
[16] S. Kondoh, U.S. Patent No. 6,750,837 (15 June 2004).
[17] L. A. Beresnev, V. G. Chigrinov, D. I. Dergachev, E. P. Poshidaev, J. Funfschilling, and M. Schadt, Liq. Cryst. **5**, 1171 (1989).
[18] M. Schadt, K. Schmitt, V. Kozinkov, and V. Chigrinov, Jpn. J. Appl. Phys. **31**, 2155 (1992).
[19] O. B. Yun, K. M. Lee, B. Y. Kim, Y. H. Kim, J. W. Han, J. M. Han, S. K. Lee, and D. S. Seo, J. Appl. Phys. **104**, 064502 (2008).
[20] M. Reznikov, Y. Reznikov, K. Slyusarenko, J. Varshal, and M. Manevich, J. Appl. Phys. **111**, 103118 (2012).
[21] A. K. Geim and K. S. Novoselov, Nat. Mater. **6**, 183 (2007).
[22] A. B. Kuzmenko, E. van Heumen, F. Carbone, and D. van der Marel, Phys. Rev. Lett. **100**, 117401 (2008).
[23] S. Ghosh, I. Calizo, D. Teweldebrhan, E. P. Pokatilov, D. L. Nika, A. A. Balandin, W. Bao, F. Miao, and C. N. Lau, Appl. Phys. Lett. **92**, 151911 (2008).
[24] A. A. Balandin, S. Ghosh, W. Bao, I. Calizo, D. Teweldebrhan, F. Miao, and C. N. Lau, Nano Lett. **8**, 902 (2008).
[25] T. Ohta, A. Bostwick, J. L. McChesney, T. Seyller, K. Horn, and E. Rotenberg, Phys. Rev. Lett. **98**, 206802 (2007).
[26] Y. U. Junga, K. W. Parka, S. T. Hura, S. W. Choia, and S. J. Kanga, Liq. Cryst. **41**, 101 (2014).
[27] A. B. Shivanandareddy, S. Krishnamurthy, V. Lakshminarayanan, and S. Kumar, Chem. Commun. **50**, 710 (2014).
[28] B. K. Kim, M. W. Jang, H. C. Park, H. M. Jeong, and E. Y. Kim, J. Polym. Sci., Part A: Polym. Chem. **50**, 1418 (2012).
[29] A. Malik, A. Choudhary, P. Silotia, A. M. Biradar, V. K. Singh, and N. Kumar, J. Appl. Phys. **108**, 124110 (2010).
[30] J. E. Kim, T. H. Han, S. H. Lee, J. Y. Kim, C. W. Ahn, J. M. Yun, and S. O. Kim, Angew. Chem., Int. Ed. **50**, 3043 (2011).
[31] Z. Xu and C. Gao, Nat. Commun. **2**, 571 (2011).
[32] B. Dan, N. Behabtu, A. Martinez, J. S. Evans, D. V. Kosynkin, J. M. Tour, M. Pasquali, and I. I. Smalyukh, Soft Matter **7**, 11154 (2011).
[33] P. Blake, P. D. Brimicombe, R. R. Nair, T. J. Booth, D. Jiang, F. Schedin, L. A. Ponomarenko, S. V. Morozov, H. F. Gleeson, E. W. Hill, A. K. Geim, and K. S. Novoselov, Nano Lett. **8**, 1704 (2008).

[34] R. Manohar, A. K. Srivastava, P. K. Tripathi, and D. P. Singh, J. Mater. Sci. **46**, 5969 (2011).
[35] K. S. Kim, Y. Zhao, H. Jang, S. Y. Lee, J. M. Kim, K. S. Kim, J. H. Ahn, P. Kim, J. Y. Choi, and B. H. Hong, Nature **457**, 706 (2009).
[36] R. R. Nair, P. Blake, A. N. Grigorenko, K. S. Novoselov, T. J. Booth, T. Stauber, N. M. R. Peres, and A. K. Geim, Science **320**, 1308 (2008).
[37] K. F. Mak, M. Y. Sfeir, Y. Wu, C. H. Lui, J. A. Misewich, and T. F. Heinz, Phys. Rev. Lett. **101**, 196405 (2008).
[38] D. P. Singh, S. K. Gupta, K. K. Pandey, S. P. Yadav, M. C. Varia, and R. Manohar, J. Non-Cryst. Solids **363**, 178 (2013).
[39] K. Skarp, I. Dahl, H. T. Lagerwal, and B. Stebler, Mol. Cryst. Liq. Cryst. **114**, 283 (1984).
[40] S. Kundu, T. Ray, S. K. Roy, W. Haase, and R. Dabrowski, Ferroelectrics **282**, 239 (2003).
[41] S. T. Lagerwall, *Ferroelectric and Antiferroelectric Liquid Crystals* (Wiley-VCH, Weinheim, 2000).
[42] L. Tang, Y. Wang, Y. Li, H. Feng, J. Lu, and J. Li, Adv. Funct. Mater. **19**, 2782 (2009).
[43] See Supplemental Material at http://link.aps.org/supplemental/10.1103/PhysRevE.90.022501 for the large relative permittivity of pristine graphene.
[44] K. S. Novoselov, A. K. Geim, S. V. Morozov, D. Jiang, M. I. Katsnelson, I. V. Grigorieva, S. V. Dubonos, and A. A. Firsov, Nature **438**, 197 (2005).
[45] S. K. Gupta, D. P. Singh, P. K. Tripathi, R. Manohar, M. C. Varia, L. K. Sagar, and S. Kumar, Liq. Cryst. **40**, 528 (2013).
[46] S. W. Hwang, D. H. Shin, C. O. Kim, S. H. Hong, M. C. Kim, J. Kim, K. Y. Lim, S. Kim, S. H. Choi, K. J. Ahn, G. Kim, S. H. Sim, and B. H. Hong, Phys. Rev. Lett. **105**, 127403 (2010).
[47] R. J. Stohr, R. Kolesov, J. Pflaum, and J. Wrachtrup, Phys. Rev. B **82**, 121408 (2010).
[48] P. A. Obraztsov, M. G. Rybin, V. Tyurnina, S. V. Garnov, E. D. Obraztsova, A. N. Obraztsova, and Y. P. Svirko, Nano Lett. **11**, 1540 (2011).